The 5th Joint International Conference on Multibody System Dynamics
June 24 – 28, 2018, Lisbon, Portugal

Numerical integration of a new set of equations of motion for a class of multibody systems using an augmented Lagrangian approach

Nikolaos Potosakis[1], Elias Paraskevopoulos[2] and Sotirios Natsiavas[3]

[1,2,3] *Department of Mechanical Engineering, Aristotle University, Thessaloniki, Greece, natsiava@auth.gr*

ABSTRACT — *Some new theoretical and numerical results are presented for a class of multibody systems subjected to equality motion constraints. The formulation is based on a new set of equations of motion, expressed as a system of second order ordinary differential equations. First, an appropriate set of penalty terms is introduced and these equations are put directly in an augmented Lagrangian form. Next, the position, velocity and momentum type quantities are assumed to be independent, leading to a three field set of equations. This set is then used as a basis for producing a new time integration scheme. The validity and efficiency of this scheme is verified by applying it to several example systems.*

1 Introduction

Research on the dynamics of mechanical systems subject to motion constraints is a traditional and favorable topic among researchers with different backgrounds (e.g., [1-4]). This is in part due to the fact that this area of Mechanics is still challenging and several theoretical aspects related to it remain unexplored and are amenable to improvement. Another driving factor is that a better understanding of the fundamentals in this area provides a stronger foundation and offers substantial help in the efforts to solve difficult engineering problems by deriving and employing new, more advanced, accurate and robust numerical techniques [3,5,6]. This in turn leads to useful design gains in many areas, including mechanisms, robotics, machinery, biomechanics, automotive and aerospace structures.

Typically, the equations of motion for this class of systems are derived and cast in the form of a set of differential-algebraic equations (DAEs) of high index. However, both the theoretical and the numerical treatment of DAEs is a delicate and difficult task [7]. For this reason, many attempts have been performed in the past in an effort to cure the problems related to a DAE modeling. Over the years, it has become apparent that many of the theoretical questions in the area of Analytical Dynamics can be answered in an illustrative and complete way by employing fundamental concepts of differential geometry [8,9]. Based on this observation, the main objective of this work is to use such concepts in order to provide a better theoretical foundation and to develop an appropriate numerical scheme for treating a class of constrained mechanical systems.

The new approach assigns appropriate inertia, damping and stiffness properties to the constraints. As a result, the equations of motion are second order ordinary differential equations (ODEs) in both the generalized coordinates and the Lagrange multipliers, related to the constraint action [10,11]. This, in turn, leads to elimination of the singularities associated with DAE or penalty formulations. As a consequence, there is no need to introduce artificial parameters for scaling and stabilization. In addition, the geometrical properties of the original manifold are kept unchanged by the additional constraints. This preserves the properties of the special curves of the manifold employed in the numerical discretization and leads to major advantages compared to previous work in the field of computational Multibody Dynamics [3,6]. In the present work, these equations are first put in a convenient

Augmented Lagrangian form by introducing appropriate penalty terms. Moreover, the position, velocity and momentum type quantities are assumed to be independent, forming a three field set of equations [12,13]. In particular, the weak velocities and the strong time derivatives of all the coordinates involved in the formulation are related through a new set of Lagrange multipliers, which represent momentum type variables. Next, the formulation developed is employed as a basis for producing a suitable time integration scheme for the class of systems examined. The validity and efficiency of this scheme was tested and illustrated by applying it to a number of characteristic example mechanical systems. Among other things, the results obtained verify that the scheme developed passes successfully all the tests related to a special set of challenging benchmark problems, involving redundant constraints or singular configurations, chosen by the multibody dynamics community [14]. In addition, the same scheme was also applied successfully to a number of large scale industrial applications.

The organization of this paper is as follows. First, the set of equations of motion governing the dynamics of an unconstrained discrete mechanical system is presented briefly in the following section. Then, similar equations arising in the presence of bilateral constraints are also presented in the third section. These equations are easily put in an Augmented Lagrangian form, by just adding suitable penalty terms. This task is performed in the fourth section. Based on this form, a temporal discretization scheme was developed and numerical results were obtained for several mechanical examples. Some characteristic numerical results are presented in the fifth section.

2 Application of Newton's law to systems with no motion constraints

This work examines a class of mechanical systems whose position is determined by a finite number of generalized coordinates $q=(q^1 \dots q^n)$, at any time instance t [1,9]. The motion of such a system can be represented by the motion of a fictitious point, say p, along a curve $\gamma=\gamma(t)$ in an n-dimensional manifold M, the configuration space of the system. Moreover, the tangent vector $\underline{v}=d\gamma/dt$ to this curve belongs to an n-dimensional vector space, the tangent space of the manifold at p, denoted by T_pM [4]. By construction, for any point p of M, a smooth coordinate map φ can be defined by $q=\varphi(p)$, acting from a neighborhood of p on M to the classical Euclidean space $\mathbb{R}^n$. Then, by adopting the usual summation convention on repeated indices [9], each tangent vector at point p, representing a generalized velocity, can be expressed in the form

$$\underline{v}(t)=v^i(t)\underline{e}_i\,, \tag{1}$$

where $\mathfrak{B}_e=\{\underline{e}_1 \quad \dots \quad \underline{e}_n\}$ is a basis for space T_pM. Likewise, one can define the dual space to T_pM, denoted by T_p^*M, with elements known as covectors. In dynamics, a covector represents a generalized momentum. Also, the correspondence between a covector $\underset{\sim}{u}^*$ and a vector $\underline{u}$ is established through the dual product

$$\underset{\sim}{u}^*(\underline{w})\equiv\langle\underline{u},\underline{w}\rangle, \quad \forall\underline{w}\in T_pM\,, \tag{2}$$

where $\langle\cdot,\cdot\rangle$ denotes the inner product of vector space T_pM [8]. In this way, to each basis $\{\underline{e}_i\}$ (with $i=1,\dots,n$) of T_pM, a dual basis $\{\underset{\sim}{e}^i\}$ can be established for T_p^*M by employing the condition $\underset{\sim}{e}^i(\underline{e}_j)=\delta^i_j$, where the last term is a Kronecker's delta. Then, when the set of coordinates is minimal, determination of the true path of motion on a manifold is based on application of Newton's second law in the form

$$\nabla_{\underline{v}}\underset{\sim}{p}^*_M=\underset{\sim}{f}^*_M\,, \tag{3}$$

where $\underline{v}$ is the tangent vector of the natural trajectory $\gamma(t)$, while $\underset{\sim}{f}^*_M=f_i\underset{\sim}{e}^i$ represents the applied force [1,9]. Then, if $\underline{v}=v^i\underline{e}_i$ and $\underset{\sim}{p}^*_M=p_i\,\underset{\sim}{e}^i$, application of Eq. (2) leads to

$$p_i=g_{ij}v^j\,, \tag{4}$$

where the quantities $g_{ij}=\langle\underline{e}_i,\underline{e}_j\rangle$ represent the components of the metric tensor at point p. These quantities are selected to coincide with the elements of the mass matrix of the system, defined through the kinetic energy. Finally, the covariant differential of the covector field $\underset{\sim}{p}^*(t)$ on M along a vector $\underline{v}$ of T_pM is evaluated by

$$\nabla_{\underline{v}}\underset{\sim}{p}^*(t) = (\dot{p}_i - \Lambda^m_{ji} p_m v^j)\underset{\sim}{e}^i . \tag{5}$$

where ∇ is the affine connection of the manifold. The components Λ^k_{ij} of the connection ∇ in the basis of T_pM are known as affinities [9].

Through the definition of a class of special covectors (called Newton covectors, see [11]) by

$$\underset{\sim}{h}^*_M \equiv \nabla_{\underline{v}}\underset{\sim}{p}^*_M - \underset{\sim}{f}^*_M \tag{6}$$

the equations of motion (3) at any point on the configuration manifold M can be put in the form

$$\underset{\sim}{h}^*_M = \underset{\sim}{0} . \tag{7}$$

Therefore, when there exist no motion constraints, it should be true that

$$\underset{\sim}{h}^*_M(\underline{w}) = 0 \quad \Rightarrow \quad \int_{t_1}^{t_2} \underset{\sim}{h}^*_M(\underline{w})dt = 0, \quad \forall \underline{w} \in T_pM \tag{8}$$

along a natural trajectory on the manifold and within any time interval $[t_1, t_2]$. Manipulation of the last integral requires application of integration by parts of the covariant derivative appearing in Eq. (6). This is achieved by employing the identity

$$\nabla_{\underline{v}}(\underset{\sim}{p}^*_M(\underline{w})) = (\nabla_{\underline{v}}\underset{\sim}{p}^*_M)(\underline{w}) + \underset{\sim}{p}^*_M(\nabla_{\underline{v}}\underline{w}),$$

which can be interpreted as a Leibniz rule on differentiation. Then, the following expression is obtained

$$\int_{t_1}^{t_2}[\nabla_{\underline{v}}(\underset{\sim}{p}^*_M(\underline{w})) - \underset{\sim}{p}^*_M(\nabla_{\underline{v}}\underline{w}) - \underset{\sim}{f}^*_M(\underline{w})]dt = 0 ,$$

which, after an integration by parts of the first term inside the integral, becomes

$$[\underset{\sim}{p}^*_M(\underline{w})]\Big|_{t_1}^{t_2} - \int_{t_1}^{t_2}[\underset{\sim}{p}^*_M(\nabla_{\underline{v}}\underline{w}) + \underset{\sim}{f}^*_M(\underline{w})]dt = 0 . \tag{9}$$

This equation represents the so called weak form of the equations of motion [15]. In essence, it constitutes an alternative way to determine the true history of the coordinates (i.e., position) and velocities of a mechanical system satisfying the law of motion, as expressed by Eq. (3) originally.

Further manipulation of the weak form given by Eq. (9) involves differentiation along the vectors $\underline{v}$ and $\underline{w}$. This requires the construction of two smooth vector fields on M. The first of these can be constructed by considering the tangent vector $\underline{v}$ at each point of the natural trajectory $\gamma(t)$. The second vector field can then be created by introducing another vector $\underline{w}$ of the tangent space at each point of the same trajectory, which can be arbitrary. Therefore, a variation of any scalar function f is defined as the derivative of f along vector $\underline{w}$, by

$$\delta f \equiv \underline{w}(f) = f_{,i}w^i .$$

Then, $w^i = \delta q^i$ for holonomic coordinates. Finally, after defining the objective function

$$\mathscr{T}_M = \tfrac{1}{2}\left\|\underset{\sim}{h}^*_M\right\|^2, \tag{10}$$

it is straightforward to show that

$$\delta\mathscr{T}_M = \underset{\sim}{h}^*_M(\underline{w}) = 0, \quad \forall \underline{w} \in T_pM ,$$

which leads to Eq. (8).

3 Application of Newton's law to systems with bilateral constraints

Next, consider a mechanical system subject to a set of k scleronomic constraints, which can be put in the form

$$\dot{\psi}(q, \underline{v}) \equiv A(q)\underline{v} = \underline{0}, \tag{11}$$

where $\underline{v}$ is a vector in the tangent space T_pM and $A=[a_i^R]$ is a known $k\times n$ matrix. In the special case where a constraint is holonomic, its equation can be integrated and written in the algebraic form

$$\phi^R(q)=0\,. \tag{12}$$

Based on the above, it was shown in an earlier study that the equations of motion of the class of systems examined can now be cast in the form

$$\underset{\sim}{h}^*\equiv\underset{\sim}{h}^*_M-\underset{\sim}{h}^*_C=\underset{\sim}{0} \tag{13}$$

on the original manifold M [11], with

$$\underset{\sim}{h}^*_M=h_i\underset{\sim}{e}^i=[(g_{ij}v^j)^{\boldsymbol{\cdot}}-\Lambda^m_{\ell i}g_{mj}v^jv^\ell-f_i]\underset{\sim}{e}^i \quad and \quad \underset{\sim}{h}^*_C=\sum_{R=1}^k h_Ra_i^R\underset{\sim}{e}^i\;, \tag{14}$$

where

$$h_R=(\bar{m}_{RR}\dot{\lambda}^R)^{\boldsymbol{\cdot}}+\bar{c}_{RR}\dot{\lambda}^R+\bar{k}_{RR}\lambda^R-\bar{f}_R\,. \tag{15}$$

In the last relation and in the sequel, the convention on repeated indices does not apply to index R. Moreover, the coefficients

$$\bar{m}_{RR}=c_R^ig_{ij}c_R^j\,,\quad \bar{c}_{RR}=-c_R^i\frac{\partial f_i}{\partial v^j}(q,\underline{v},t)c_R^j\,,\quad \bar{k}_{RR}=-c_R^i\frac{\partial f_i}{\partial q^j}(q,\underline{v},t)c_R^j \quad \text{and} \quad \bar{f}_R=c_R^if_i(q,\underline{v},t)\,, \tag{16}$$

represent an equivalent mass, damping, stiffness and forcing quantity, respectively, obtained through a projection along a special direction $\underline{c}_R$ on T_pM [11]. Specifically, the components of the n-vector $\underline{c}_R$ are selected to satisfy

$$a_i^Rc_R^i=1\,. \tag{17}$$

To compare with existing formulations, matrix notation is employed next, with

$$\underline{q}=(q^1\;\cdots\;q^n)^T\,,\quad \underline{\lambda}=(\lambda^1\;\cdots\;\lambda^k)^T\,,\quad M=[g_{ij}] \quad \text{and} \quad \underline{f}(t)=(f_1\;\cdots\;f_n)^T\,.$$

Then, Eq. (13) can be put in the general form

$$(M(\underline{q})\dot{\underline{q}})^{\boldsymbol{\cdot}}+\underline{h}(\underline{q},\dot{\underline{q}})=\underline{f}(t)+A^T(\underline{q})[(\bar{M}\dot{\underline{\lambda}})^{\boldsymbol{\cdot}}+\bar{C}\dot{\underline{\lambda}}+\bar{K}\underline{\lambda}-\bar{\underline{f}}]\,, \tag{18}$$

where the term $\underline{h}(\underline{q},\dot{\underline{q}})$ arises in the presence of nonzero affinities on the original manifold M and includes the classical quadratic velocity terms [5], while the elements of the diagonal matrices

$$\bar{M}=diag(\bar{m}_{11}\;\cdots\;\bar{m}_{kk})\,,\quad \bar{C}=diag(\bar{c}_{11}\;\cdots\;\bar{c}_{kk}) \quad \text{and} \quad \bar{K}=diag(\bar{k}_{11}\;\cdots\;\bar{k}_{kk})$$

and array $\bar{\underline{f}}$ are determined by Eq. (16). The major difference with the classical approaches lies in the last term of Eq. (18), representing the constraint forces. Specifically, in all current analytical formulations, only the “static” term $A^T\underline{\lambda}$ appears in its place, so that the equations of motion are cast in the form

$$M(\underline{q})\ddot{\underline{q}}=\underline{g}(\underline{q},\dot{\underline{q}},t)+A^T(\underline{q})\underline{\lambda}\,,$$

with

$$\underline{g}(\underline{q},\dot{\underline{q}},t)=\underline{f}(t)-\underline{h}(\underline{q},\dot{\underline{q}},t)-\dot{M}(\underline{q})\dot{\underline{q}}\,.$$

Equation (18) represents a set of n second order coupled ODEs in the $n+k$ unknowns q^i and λ^R. The cases involving quasi-coordinates are also covered by the same equations [15,16]. Moreover, the additional information needed for a complete mathematical formulation is obtained by incorporating the k equations of the constraints, which are expressed originally by Eq. (11). In particular, for each holonomic or non-holonomic constraint, a second order ODE is obtained, with form

$$g_R\equiv(\bar{m}_{RR}\dot{\phi}^R)^{\boldsymbol{\cdot}}+\bar{c}_{RR}\dot{\phi}^R+\bar{k}_{RR}\phi^R=0 \quad or \quad g_R\equiv(\bar{m}_{RR}\dot{\psi}^R)^{\boldsymbol{\cdot}}+\bar{c}_{RR}\dot{\psi}^R=0\,, \tag{19}$$

respectively, for $R=1,\ldots,k$. These conditions have a similar but more general form than those employed in the so-called Baumgarte stabilization [3,6]. In addition, these equations were derived as part of a systematic approach and were not introduced artificially. Also, all the coefficients of these equations were determined analytically and not selected through an adhoc selection.

The present approach brings a major theoretical advantage when compared to other approaches applied so far in the field of Analytical Dynamics and Multibody Dynamics in particular [11]. This is related to a physically consistent and correct elimination of the singularities associated with the sets of DAEs of motion. Specifically, the introduction of the Lagrange multipliers associated to the motion constraints is based on a dynamic treatment of the constraint equations, which is consistent with that of the main equations of motion. As a result, the derivatives of the Lagrange multipliers appear naturally in these equations and there is no reason for performing extra differentiations of the constraint equations. In addition, there is no need for an arbitrary and externally imposed numerical stabilization. Furthermore, all the constraints are introduced automatically and possess a proper numerical scaling, in contrast to current penalty formulations, which are based on an adhoc introduction of terms and selection of parameters [3,6].

4 A new numerical scheme for systems with bilateral constraints

In analogy to Eq. (10) and taking into account the motion constraints expressed by Eq. (11) or Eq. (19), alternatively, define next the function $\mathscr{T}_M$ gives its place to

$$\mathscr{T}_A = \tfrac{1}{2}\left\|\underset{\sim}{h}^*\right\|^2 - \tfrac{1}{2}\left\|\underset{\sim}{h}_\rho^*\right\|^2 . \tag{20}$$

The new function is augmented by the norm of the covector

$$\underset{\sim}{h}_\rho^* = \sum_{R=1}^{k} \rho_R g_R (a_i^R \underset{\sim}{e}^i) , \tag{21}$$

including the penalty factors ρ_R. Then, it is easy to show that the above definitions lead to

$$\delta\mathscr{T}_A = (\underset{\sim}{h}^* - \underset{\sim}{h}_\rho^*)(\underline{w}) = 0, \quad \forall \underline{w} \in T_p M ,$$

which is equivalent to minimizing the function $\left\|\underset{\sim}{h}^*\right\|^2$, where the quantity $\underset{\sim}{h}^*$ is defined through Eq. (13), subject to the motion constraints defined by Eq. (19). Eventually, this leads to

$$\int_{t_1}^{t_2} (\underset{\sim}{h}_M^* - \underset{\sim}{h}_C^*)(\underline{w})dt + \int_{t_1}^{t_2} \underset{\sim}{h}_\rho^*(\underline{w})dt = 0, \quad \forall \underline{w} \in T_p M . \tag{22}$$

The last form, known as a weak form of the equations of motion, is also complemented by the following terms

$$\int_{t_1}^{t_2} g_R \delta\lambda^R dt = 0 , \tag{23}$$

for each motion constraint and arbitrary multipliers $\delta\lambda^R$.

In a weak formulation, it is frequently advantageous to consider the position, velocity and momentum variables as independent quantities [15]. For this, a new velocity field $\underline{\hat{v}}$ is introduced on manifold M, which should eventually be forced to become identical to the true velocity field $\underline{v}$ through the action of an arbitrary covector with components $\delta \hat{p}_i$. A similar action can be taken for the velocity type components $\mu^R \equiv \dot{\lambda}^R$, by introducing another vector field with components $\hat{\mu}^R$ and a new set of multipliers, $\delta\hat{\pi}_R$, with $R=1,\ldots,k$. Likewise, one can relate the variations in the strong time derivatives v^i and μ^R of the position type variables to those of the weak velocities, $\hat{v}^i$ and $\hat{\mu}^R$, through two new sets of Lagrange multipliers, denoted by $\hat{p}_i$ and $\hat{\pi}_R$, respectively. To achieve these tasks, the weak form expressed by Eqs (22) and (23) should be augmented by the terms

$$\int_{t_1}^{t_2} [\hat{p}_i(\delta\hat{v}^i - \delta v^i) + \delta\hat{p}_i(\hat{v}^i - v^i)]dt = 0 \quad and \quad \int_{t_1}^{t_2} [\hat{\pi}_R(\delta\hat{\mu}^R - \delta\mu^R) + \delta\hat{\pi}_R(\hat{\mu}^R - \mu^R)]dt = 0 . \tag{24}$$

Finally, by adding up all these terms and performing appropriate mathematical operations, including the usual integration by parts step, it yields eventually the following three field set of equations

$$\begin{aligned}&(p_i-\sum_{R=1}^{k}a_i^R\overline{m}_{RR}\overline{\mu}^R)w^i\Big|_{t_1}^{t_2}+\sum_{R=1}^{k}\overline{m}_{RR}\dot{\phi}^R\delta\lambda^R\Big|_{t_1}^{t_2}+\int_{t_1}^{t_2}[\delta\hat{p}_i(\hat{v}^i-v^i)+\sum_{R=1}^{k}\delta\hat{\pi}_R(\hat{\mu}^R-\mu^R)]dt\\&+\int_{t_1}^{t_2}[(-p_i+\sum_{R=1}^{k}a_i^R\overline{m}_{RR}\overline{\mu}^R+\hat{p}_i)\delta\hat{v}^i+\sum_{R=1}^{k}(\hat{\pi}_R-\overline{m}_{RR}\dot{\phi}^R)\delta\hat{\mu}^R]dt-\int_{t_1}^{t_2}(\hat{p}_i\delta v^i+\sum_{R=1}^{k}\hat{\pi}_R\delta\mu^R)dt\\&+\int_{t_1}^{t_2}\{f_i+\sum_{R=1}^{k}[(\overline{c}_{RR}\overline{\mu}^R+\overline{k}_{RR}\overline{\lambda}^R-\overline{f}_R)a_i^R-\overline{m}_{RR}\mu^R\tfrac{Da_i^R}{Dt}]\}w^i\,dt+\sum_{R=1}^{k}\int_{t_1}^{t_2}(\overline{c}_{RR}\dot{\phi}^R+\overline{k}_{RR}\phi^R)\delta\lambda^R dt=0,\end{aligned}\tag{25}$$

where the variations w^i, $\delta\lambda^R$, $\delta\hat{v}^i$, $\delta\hat{\mu}^R$, $\delta\hat{p}_i$ and $\delta\hat{\pi}_R$ are independent for all $i=1,\ldots,n$ and $R=1,\ldots,k$, while

$$\tfrac{Da_i^R}{Dt}=\dot{a}_i^R-\Lambda_{ji}^{\ell}a_\ell^R\hat{v}^j\,,\quad \overline{\mu}^R=\hat{\mu}^R+\rho_R\dot{\phi}^R\quad and\quad \overline{\lambda}^R=\hat{\lambda}^R+\rho_R\phi^R\,.\tag{26}$$

Equation (25) is the final weak form obtained for the class of constrained mechanical systems examined. This form is convenient for performing an appropriate numerical discretization of the equations of motion, leading to improvements over existing numerical schemes based on advanced analytical tools. For the purposes of the present work, this form was also put within the framework of an augmented Lagrangian formulation [17-21]. This method is appropriate for performing a geometrically exact discretization.

In brief, after assuming consistent polynomial expansions, a set of nonlinear algebraic equations is obtained for the unknowns of the problem, which consist of q^i, λ^R, $\hat{v}^i$, $\hat{\mu}^R$, $\hat{p}_i$ and $\hat{\pi}_R$. This set is solved by a block-type iterative technique within each time step, according to the following scheme. First, assume that the values of all the unknowns but $\hat{v}^i$ are fixed. After solving for the new values of the velocities $\hat{v}^i$ the subsystem of the algebraic equations resulting by the terms in the weak form multiplied by δq^i (for holonomic coordinates) and $\delta\lambda^R$, an appropriate augmentation is performed leading to the new values of $\hat{\mu}^R$, based on Eq. (26). Then, the values of the coordinate variables q^i and λ^R are determined through a direct update, resulting by the terms of the weak form multiplied by $\delta\hat{p}_i$ and $\delta\hat{\pi}_R$. Finally, the updated values of the momentum variables $\hat{p}_i$ and $\hat{\pi}_R$ can be obtained by using the subsystem resulting by the terms of the weak form multiplied by $\delta\hat{v}^i$ and $\delta\hat{\mu}^R$.

5 Numerical results

The numerical scheme developed leads to a full exploration of the major advantages of the theoretical method applied, in a quite natural manner. It is especially useful when the configuration space of the system possesses group properties [22,23]. The success of this formulation was demonstrated by the accurate solution obtained for a number of challenging problems. Some characteristic results are presented next for several typical examples. The first ones have a relatively simple geometry and are of academic interest, while the last example was taken from an industrial application.

5.1 Plane Pendulum

The first set of numerical results refers to a planar pendulum, composed of a particle with mass $m=1\,kg$, attached to one end of a massless rigid rod with length $L=1\,m$. The other end of the rod is connected to the ground through a revolute joint so that the system motion is confined to take place in the x-y plane. This pendulum is released from rest, from an initial position, shown in Fig. 1a. Consequently, it undergoes large amplitude oscillations, due to the action of gravity along the negative Y direction.

In Figs 1b-1d are presented and compared numerical results obtained by the new solver (labeled by LMD) with results obtained from a state of the art code, employing a solver based on backward differentiation formulas (BDF) [24]. In both cases, an effort was made to keep the same time step and accuracy level in the numerical calculations. In particular, an accuracy level of 0.01 was required in all runs, using either code.

First, in Fig. 1b is shown the mechanical energy of the system as a function of time, assuming a zero potential energy at the position shown in Fig. 1a. Clearly, the results obtained by the commercial code exhibit a gradual and substantial mechanical energy loss. This is probably related to the high level of artificial damping induced in the

BDF scheme employed. The consequences of this effect are demonstrated in Figs 1c and 1d, presenting the time history of the vertical component of the displacement of the particle at the beginning and at a later time interval of the oscillation. The results indicate a drift and a reduction in the amplitude of oscillation obtained by the BDF method. It is important to note that a similar behavior with [24] was also observed by employing another state of the art code in multibody dynamics, which uses also a BDF scheme [25].

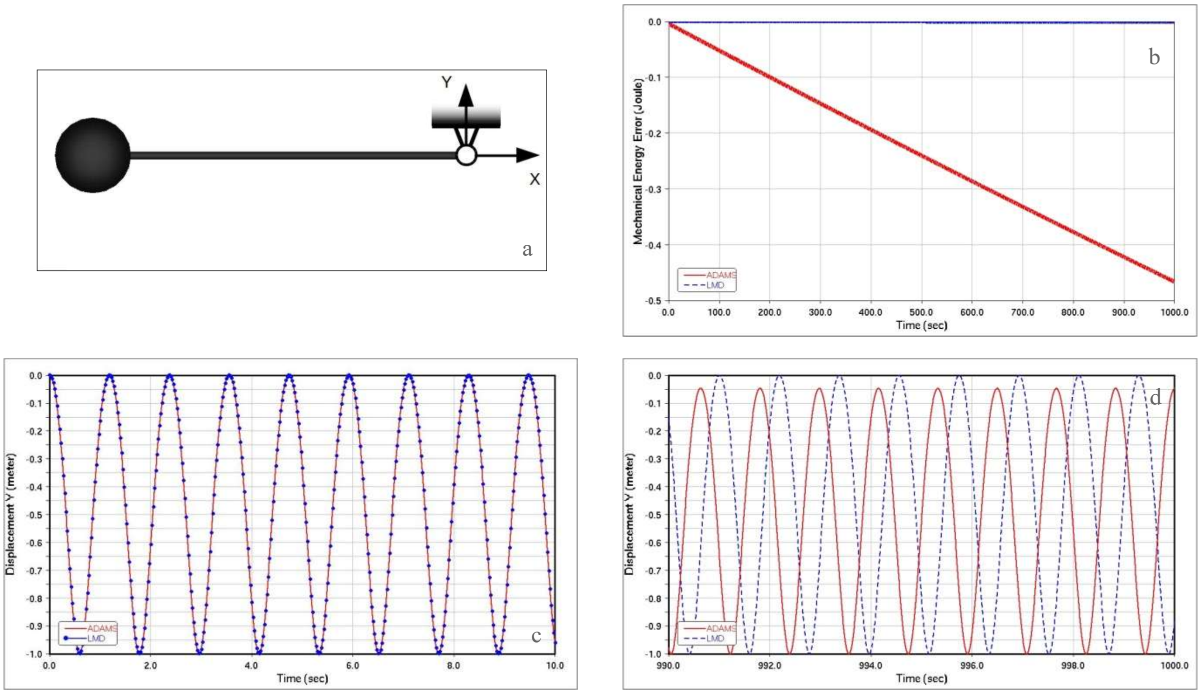

Fig. 1: Numerical results for a planar pendulum: (a) mechanical model, (b) mechanical energy error, (c)/(d) history of the particle vertical displacement at the beginning and at a later period of time.

The good performance of the new code is due to the fact that the new set of equations of motion employed includes suitable terms, avoiding a growth in the constraint violation error in an automatic manner. For instance, in Fig. 2a are shown results obtained by the new code, by taking into account the critical term $\overline{m}_{RR}$, evaluated by Eq. (16), or setting it to a different value in the calculations, i.e., $\overline{m}_{RR}/10$, $\overline{m}_{RR}/100$ or 0. As it is obvious from Eqs (14) and (15), this term assures the presence of the constraint inertia term $\ddot{\lambda}^R$ in the equations of motion. Obviously, an incorrect choice or elimination of this term leads to a dramatic reduction of the time step, causing a sudden termination of the numerical calculations. In all cases, the initial penalty values were chosen to be equal to 100. In Fig. 2b are shown the changes in the values of the penalty factors leading to convergence in the case with $\overline{m}_{RR}/10$. Obviously, the penalty factors change with time and are different for each constraint. For the correct value of $\overline{m}_{RR}$, the step size was found to remain constant in all cases examined for the specific example, as shown in Fig. 2c. Likewise, the penalty values remained also constant, as is shown in Fig. 2d, while the violation of the constraint was limited to very low levels, as indicated by the results of Fig. 2e. Finally, Fig. 2f shows results for three cases, corresponding to $\overline{m}_{RR}/10$, where the penalty factors are kept constant throughout the simulations. For the larger penalty value the correct solution is obtained without a reduction in the time step. For the intermediate penalty value a solution is reached, after an order of magnitude reduction of the time step. The smallest penalty value leads to a drastic reduction of the time step and termination of the solution process. These results are expected to worsen in more complicated examples, where the values of the $\overline{m}_{RR}$ are not constant.

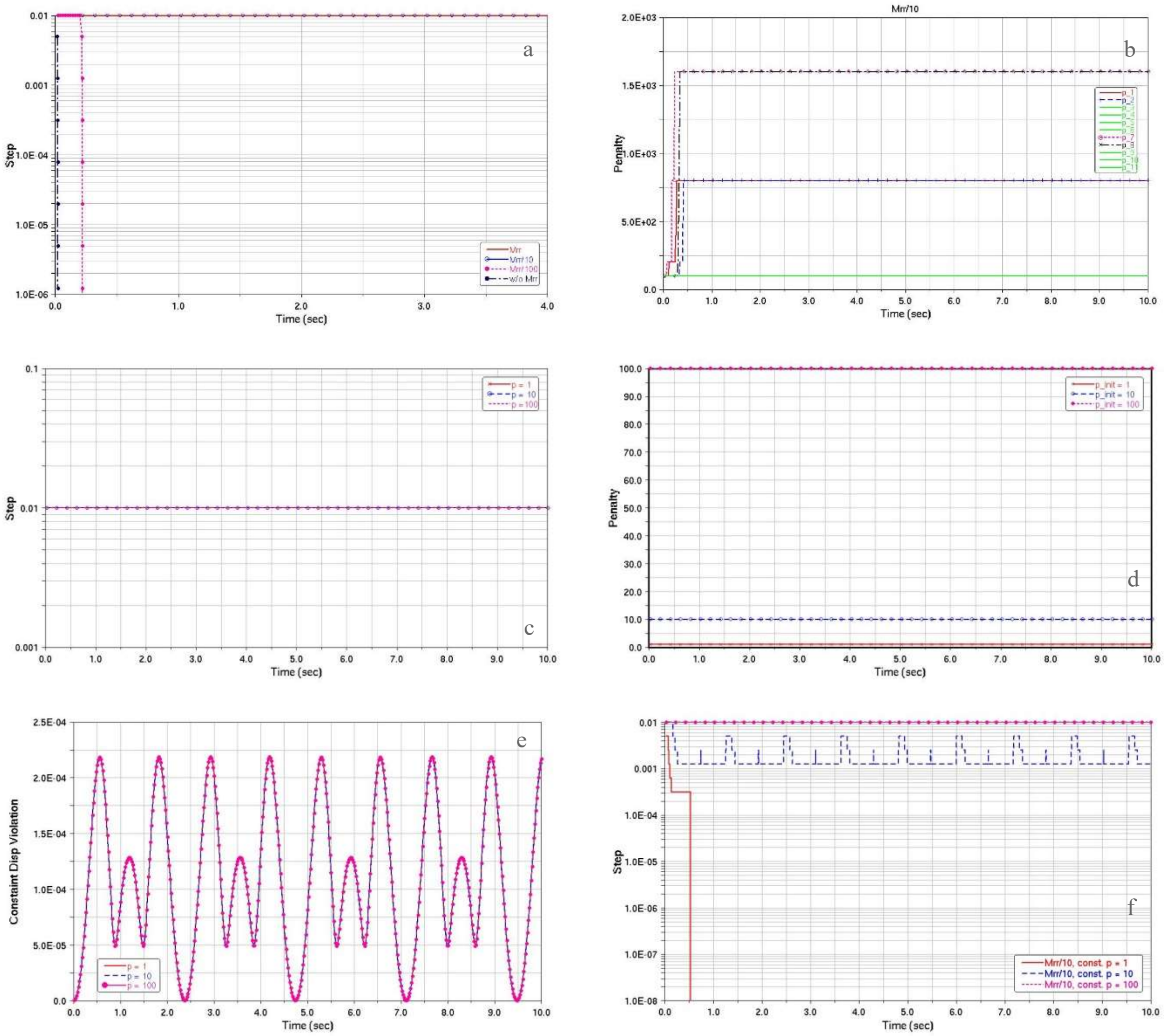

Fig. 2: Numerical results for a planar pendulum: (a) time step as a function of time for different fraction values of $\bar{m}_{RR}$ (all initial penalty values are equal to 100), (b) changes in the values of the penalty factors leading to convergence in case with $\bar{m}_{RR}/10$, (c) step size for the correct value of $\bar{m}_{RR}$, (d) penalty values for the correct value of $\bar{m}_{RR}$, (e) violation of the constraint for the correct value of $\bar{m}_{RR}$, (f) step size for constant penalty factors and $\bar{m}_{RR}/10$.

5.2 Double Four Bar Mechanism

Next, in Fig. 3 are compared results obtained by applying the new method with similar results obtained for a typical benchmark problem [14]. In brief, the double four bar mechanism examined is a representative of a multibody system passing through a singular configuration. All the rods have equal length and uniformly distributed mass. Specifically, when the bars reach the horizontal position, the number of degrees of freedom increases instantaneously from one to three. In the set of calculations presented next, the mechanism starts from rest from the position shown in Fig. 3a and executes oscillations due to the action of gravity along the –y direction. Again, the results of the new method are labeled by LMD.

First, the results of Fig. 3b verify the closeness of the results obtained by the two methods, within the time interval considered. However, the results presented in Fig. 3c demonstrate a difference in the error in the mechanical energy (taking as a reference configuration the one shown in Fig. 3a). The new method predicts a constant value close to zero, which is the exact value. In addition, the results shown in Figs 3d, 3e and 3f show three different types of failure in the response obtained by using the same BDF solver as in the previous example

[24]. More specifically, the simulation stops suddenly (Fig. 3d), the solver finds a wrong solution (Fig. 3e) or it predicts a breaking of the connections leading to a disassembling of its members (Fig. 3f), as the mechanism passes from the singular position.

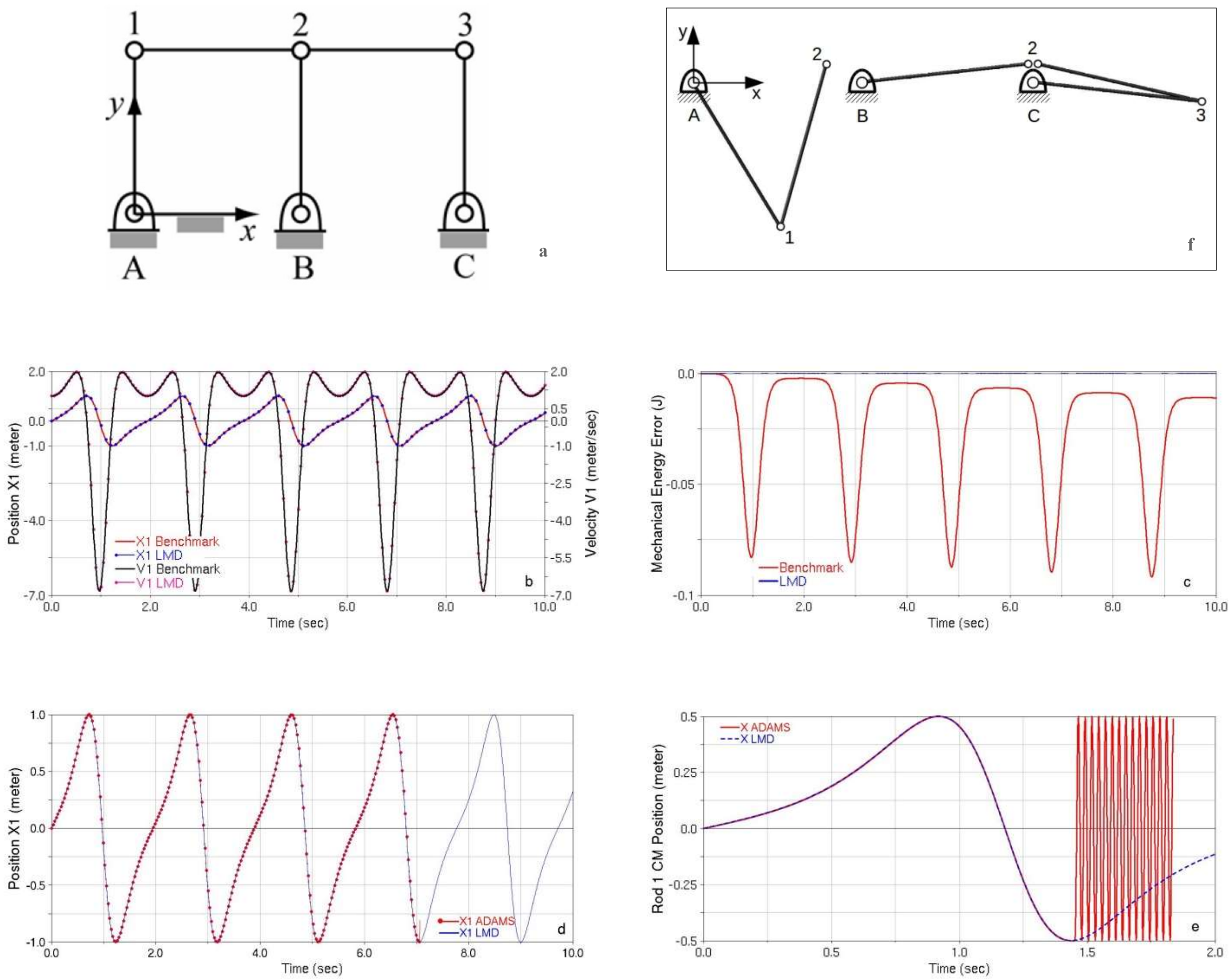

Fig. 3: Numerical results for a double four bar mechanism: (a) mechanical model, (b) history of position and velocity of point P_1 of the mechanism, (c) mechanical energy error, ADAMS results (using a BDF method) where (d) simulation stops, (e) solver finds a wrong solution and (f) the mechanism breaks.

5.3 Rectangular Bricard Mechanism

The next set of results refers to a six-bar rectangular Bricard mechanism, shown in Fig. 4a. All the rods are connected with revolute joints, have equal length and uniformly distributed mass. Again, this system moves due to gravity acting along the negative y-axis. The mechanism examined represents a mechanical system which is redundantly constrained throughout its motion and, due to this property, it also belongs to a special set of benchmark problems [14].

First, in Fig. 4b are shown the time histories of the x, y and z coordinates of point P_2, while in Fig. 4c is depicted the mechanical energy of the system. Finally, in Figs 4d and 4e are presented the corresponding histories of the constraint violations in the position and velocity levels during the same time interval, represented by the norm of the array of the constraints at each level.

Direct comparison of the results in Fig. 4 illustrates that the present method is accurate and passes successfully the benchmark tests. It also presents an improved numerical performance. For instance, the mechanical energy computed by the present method remains virtually constant (Fig. 4c). In addition, the errors in both the displacement and velocity constraint violations are bounded and stay at the same level, throughout the time interval examined (Figs 4d and 4e).

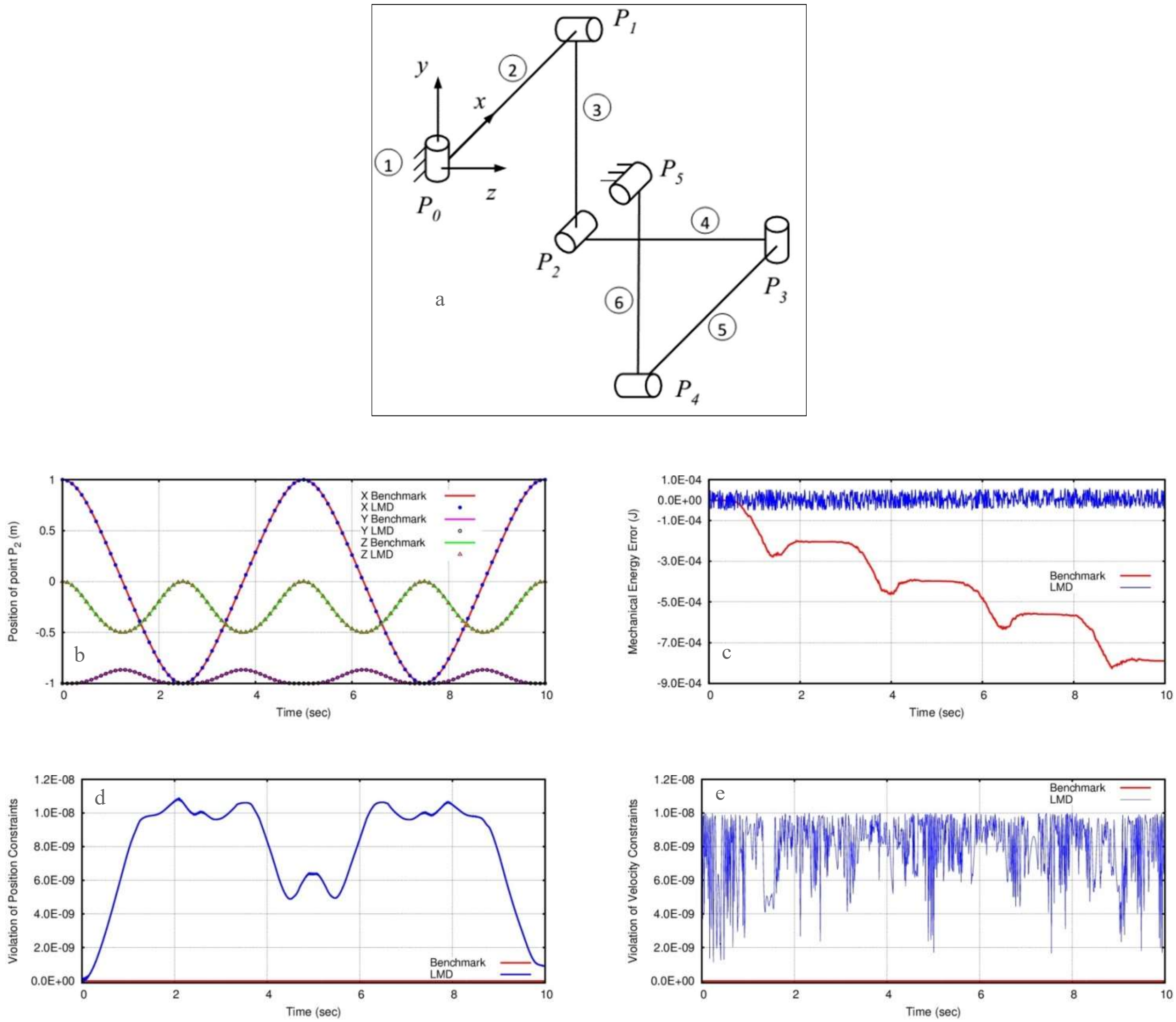

Fig. 4: (a) Mechanical model of a Bricard mechanism, (b) history of the x, y and z coordinates of point P_2, (c) mechanical energy, (d) violation of position and (e) violation of velocity constraints.

5.4 Flyball Governor

The next example is a flyball governor, shown in Fig. 4a. Here, the coupler rods have been replaced by spring-damper elements with stiffness and damping coefficients equal to $k = 8\cdot 105$ N/m and $c = 4\cdot 104$ Ns/m, respectively. This produces a stiff system and is included in a special set of benchmark problems [14]. At time t = 0, both arms form an angle β = 30º with respect to the *x*-axis and the shaft rotates about its axis with an angular velocity ω = 2π rad/s. Subsequently, the system moves under a gravitational force along the negative z axis.

First, in Figs 5b and 5c are compared results of the new method with a benchmark solution for the history of the angular velocity and the distance s, respectively. The results indicate a good level of agreement. Finally, in Figs 5d and 5e are shown results for the numerical violation observed in the position and velocity constraint, respectively. Clearly, the level of both of these errors is quite low and is controlled by the new methodology developed in an automatic way.

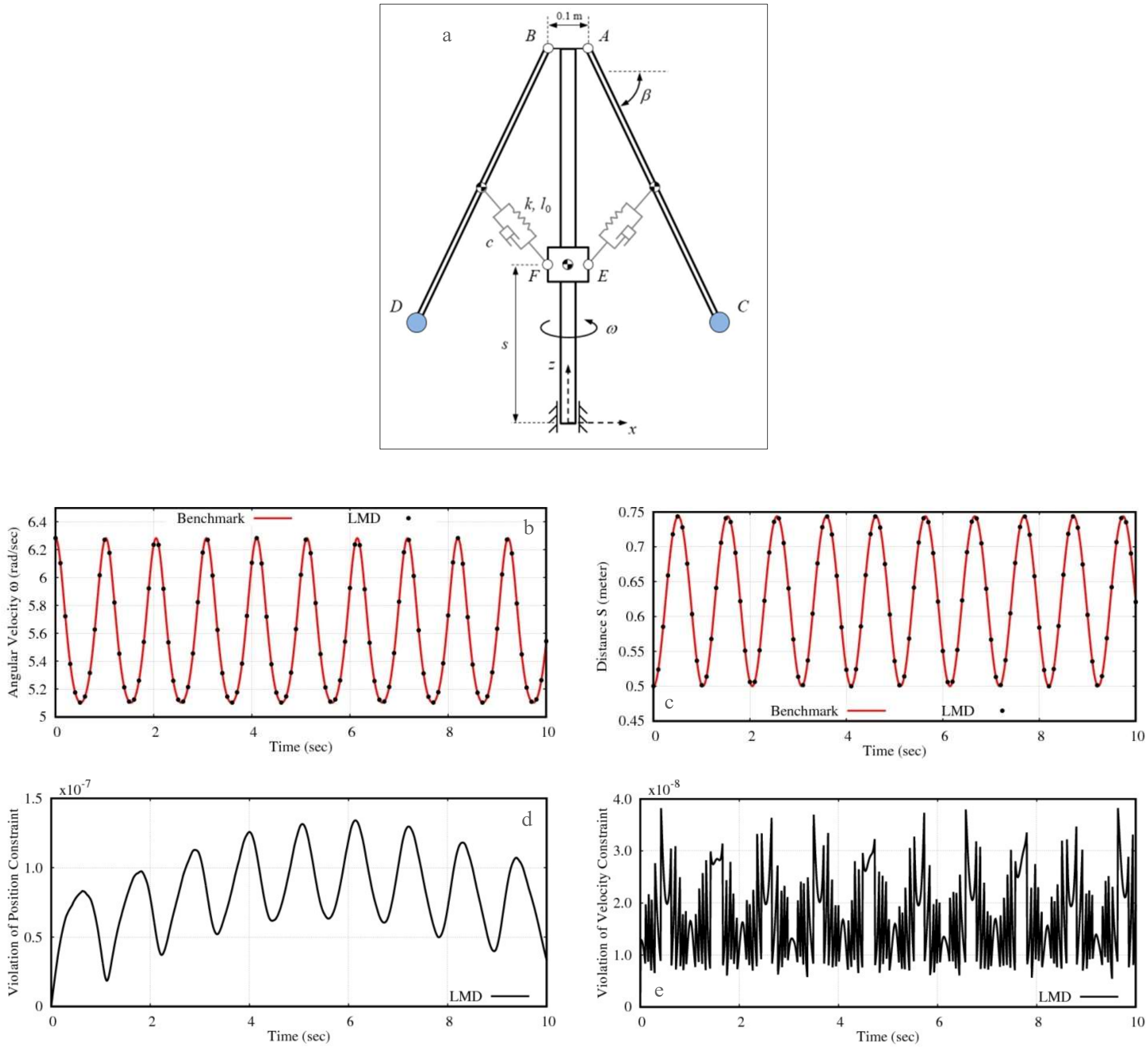

Fig. 5: Numerical results for a flyball governor: (a) mechanical model, (b) history of the angular velocity of shaft, (c) distance S, (d)/(e) violation of constraints in position and velocity field, respectively

5.5 Rolling Sphere on a Turntable

The system examined next consists of a sphere rolling over a turntable, as shown in Fig. 6a. The special feature of this problem is that it belongs to the class of systems subject to rheonomic constraints. This problem has a long history. For instance, even analytical solutions are available for horizontal and tilted turntables, under pure rolling conditions [26]. Here, a steel ball with a radius of $R = 2{,}5\ cm$ is considered, moving on a horizontal rotating disk. The ball starts at the center of the turntable with a small initial velocity $\underset{\sim}{v}_0 = \begin{pmatrix} 0.5 & -0.5 & 0 \end{pmatrix}^T m/s$ and rolls without sliding, while the disk rotates with a constant angular velocity $\Omega_Z = 2\pi\, rad/\mathrm{s}$ along the vertical axis Z. In Fig. 6b is presented the trajectory obtained for the ball by applying the existing analytical results and the new method developed. As expected by the choice of parameters, the path is circular, while the speed remains constant throughout the whole trajectory.

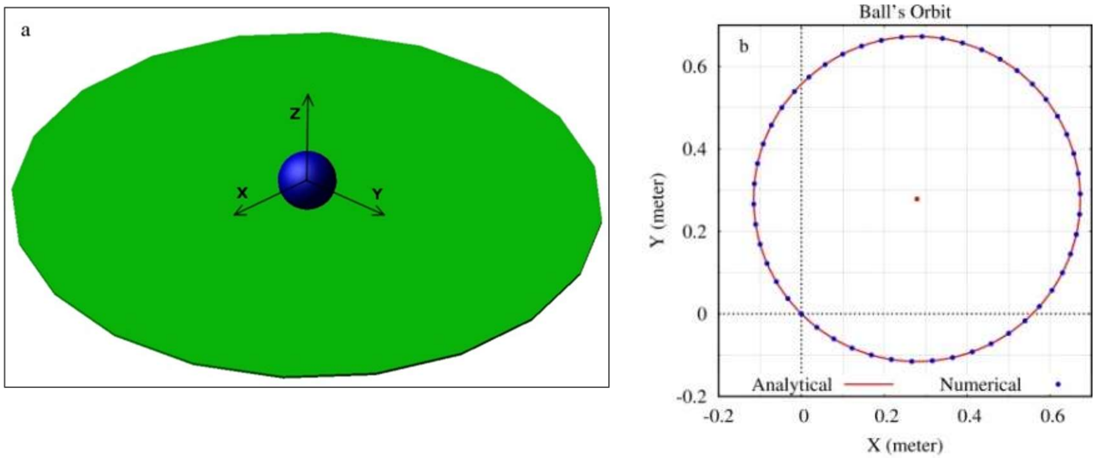

Fig. 6: Numerical results for the rolling ball model: (a) mechanical model and (b) orbit of the ball.

5.6 Complex Model of a Ground Vehicle

In the last example, a quite complex model of a ground vehicle is examined, shown in Fig. 7a. This model is composed of a basic powertrain system, a complex steering system, together with involved front and rear suspension systems with jounce and rebound bumpers. Also, the tires were modeled using the well-known Pacejka tire model [27]. In total, the model consists of 53 rigid bodies, interconnected with 49 kinematical constraints, 29 bushings, 9 spring-damper systems and 9 action-reaction force elements. As a consequence, the total number of degrees of freedom of the final model is 134. In the examples examined, the vehicle is subjected to two classical road handling tests. For this, an appropriate driving torque and steering angle is applied at the car's differential and wheel during the motion, as shown in Figs 7b and 7c. In the first test, the vehicle is running over a straight path with a constant longitudinal velocity $V_X \approx -60\ km/h$ before it starts performing a typical double lane change (DLC). In Figs 7d and 7f are presented selected results obtained for tire forces and velocity components by applying the new numerical method (labeled by LMD). Moreover, these results are compared with results obtained for the same model by two state of the art numerical codes [24,25]. These codes set up the equations of motion and solve them numerically as a system of DAEs. In the second test, a swept steering maneuver is performed. Typical results for tire forces and velocity components are shown and compared in Figs 7e and 7g. The differences appearing between the results obtained by the new method and one of the codes [25] is most probably due to differences in the tire models employed.

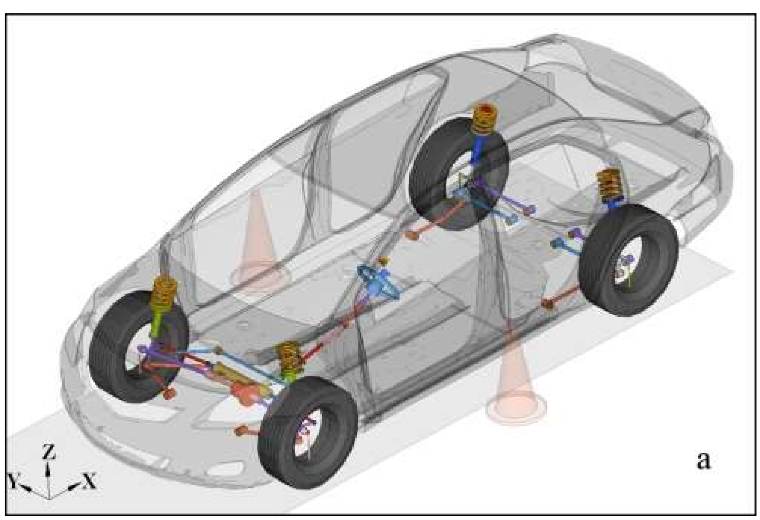

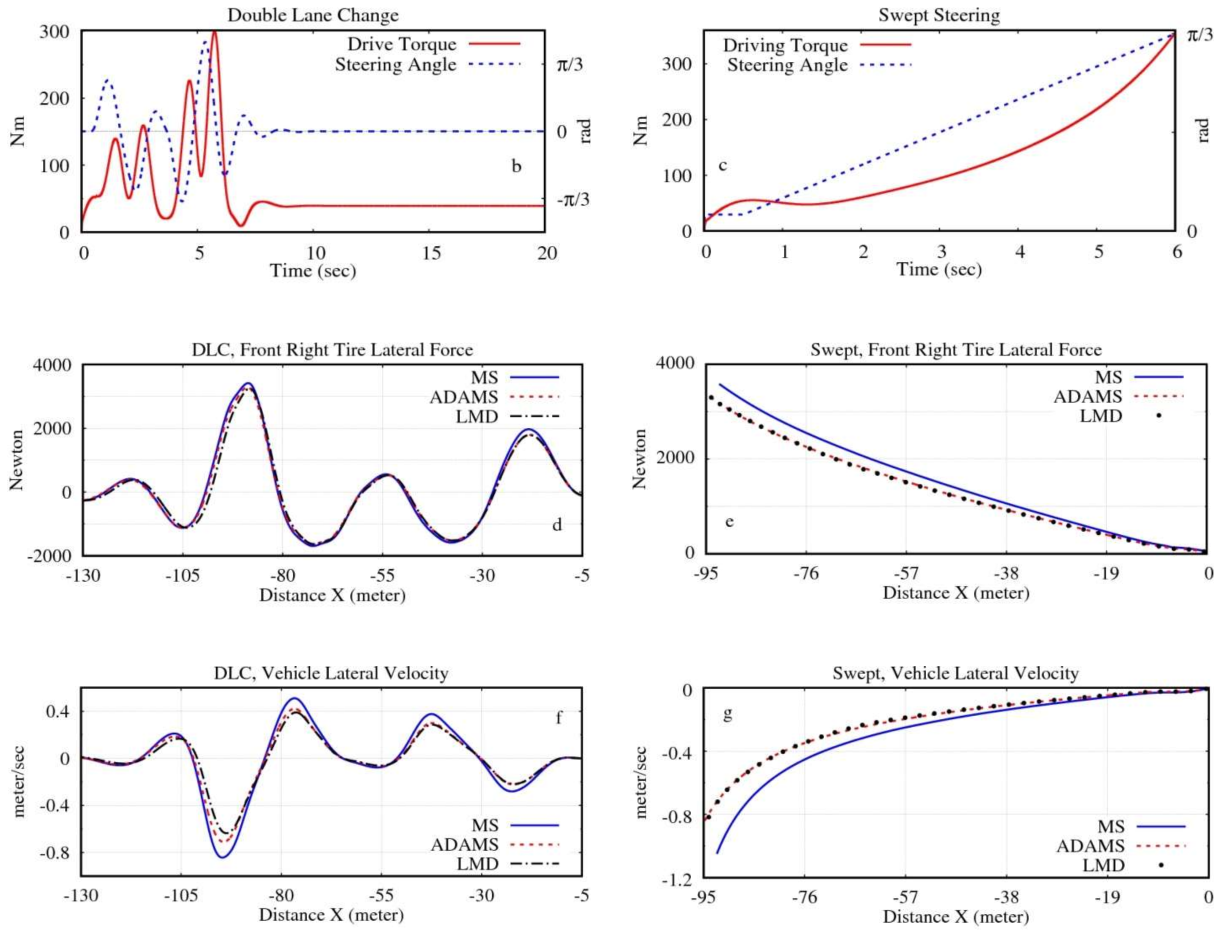

Fig. 7: Numerical results for a car model: (a) vehicle model, (b)/(c) driving torque and steering angle input curves, (d)/(f) front right tire lateral force and vehicle lateral velocity for the DLC analysis, (e)/(g) front right tire lateral force and vehicle lateral velocity for the swept test analysis.

References

[1] D.T. Greenwood, *Principles of Dynamics*, Prentice-Hall Inc., Englewood Cliffs, New Jersey, 1988.

[2] R.M. Murray, Z. Li and S.S. Sastry, *A Mathematical Introduction to Robot Manipulation*, CRC Press, Boca Raton, Florida, . 1994.

[3] M. Geradin and A. Cardona, *Flexible Multibody Dynamic,* John Wiley & Sons, New York, 2001.

[4] A.M. Bloch, *Nonholonomic Mechanics and Control*, Springer-Verlag, New York, . 2003.

[5] A.A. Shabana, *Dynamics of Multibody Systems*, third ed. Cambridge University Press, New York, 2005.

[6] O.A. Bauchau, *Flexible Multibody Dynamics*, Springer Science+Business Media, London, 2011.

[7] K.E. Brenan, S.L. Campbell and L.R. Petzhold, *Numerical Solution of Initial-Value Problems in Differential-Algebraic Equations*, North-Holland, New York, 1989.

[8] J.E. Marsden and T.S. Ratiu, *Introduction to Mechanics and Symmetry*, second ed. Springer Science+ Business Media Inc., New York, 1999.

[9] J.G. Papastavridis, *Tensor Calculus and Analytical Dynamics*, CRC Press, Boca Raton, 1999.

[10] E. Paraskevopoulos and S. Natsiavas, "On application of Newton's law to mechanical systems with motion constraints," *Nonlinear Dynamics*, vol. 72, pp. 455-475, 2013.

[11] S. Natsiavas and E. Paraskevopoulos, "A set of ordinary differential equations of motion for constrained mechanical systems," *Nonlinear Dynamics*, vol. 79, pp. 1911-1938, 2015.

[12] K. Rektorys, *Variational Methods in Mathematics, Science and Engineering*, D. Reidel Publishing Company, Dordrecht, 1977.

[13] A. Ženišek, Nonlinear Elliptic and Evolution Problems and their Finite Element Approximations, Academic Press, London, 1990.

[14] IFToMM T.C. for Multibody Dynamics, Library of Computational Benchmark Problems, http://www.iftomm-multibody.org/benchmark

[15] E. Paraskevopoulos and S. Natsiavas, "Weak formulation and first order form of the equations of motion for a class of constrained mechanical systems," *Int. J. Non-linear Mech.*, vol. 77, pp. 208-222, 2015.

[16] J.I. Neimark and N.A. Fufaev, *Dynamics of Nonholonomic Systems*, Translations of Mathematical Monographs, American Mathematical Society, vol. 33, 1972.

[17] J. Nocedal and S.J. Wright, *Numerical Optimization,* Springer Series in Operations Research, New York, 1999.

[18] E. Bayo and R. Ledesma, "Augmented Lagrangian and mass-orthogonal projection methods for constrained multibody dynamics," *Nonlinear Dynamics*, vol. 9, pp. 113–130, 1996.

[19] W. Blajer, "Augmented Lagrangian formulation: geometrical interpretation and application to systems with singularities and redundancy," *Mulibody System Dynamics*, vol. 8, pp. 141–159, 2002.

[20] D. Dopico, F. Gonzalez, J. Cuadrado and J. Kovecses, "Determination of holonomic and nonholonomic constraint reactions in an index-3 augmented Lagrangian formulation with velocity and acceleration projections," *ASME Journal of Computational and Nonlinear Dynamics*, vol. 9, p. 041006, 2014.

[21] F. Gonzalez, D. Dopico, R. Pastorino and J. Cuadrado, "Behaviour of augmented Lagrangian and Hamiltonian methods for multibody dynamics in the proximity of singular configurations," *Nonlinear Dynamics*, vol. 85, pp. 1491–1508, 2016.

[22] O. Brüls, A. Cardona and M. Arnold, "Lie group generalized-α time integration of constrained flexible multibody systems," *Mechanism and Machine Theory,* vol. 48, pp. 121-137, 2012.

[23] E. Paraskevopoulos and S. Natsiavas, "A new look into the kinematics and dynamics of finite rigid body rotations using Lie group theory," *Int. J. Solids Struct*., vol. 50, pp. 57-72, 2013.

[24] MSC ADAMS 2016, *User Guide*, MSC Software Corporation, California, USA.

[25] MotionSolve v14.0, *User Guide*, Altair Engineering Inc., Irvine, California, USA.

[26] K. Weltner, "Stable circular orbit of freely moving balls on rotating disks," *Am. J. Phys.*, vol. 47, pp. 984-986, 1979.

[27] H.B. Pacejka, *Tyre and Vehicle Dynamics*, third ed. Butterworth-Heinemann, 2012.